Hydrogeology Journal
https://doi.org/10.1007/s10040-024-02805-y

PAPER

# Estimation of groundwater flux with active distributed temperature sensing and the finite volume point dilution method: a field comparison

**Nataline Simon**[1] · **Laura Balzani**[1] · **Pierre Jamin**[1,2] · **Serge Brouyère**[1]

Received: 22 November 2023 / Accepted: 1 June 2024


**Abstract**
Considering the importance of characterizing groundwater flow for assessing recharge and contaminant transport, this study investigates the potential of two field methods to estimate groundwater fluxes in consolidated aquifers. To accomplish this, both the finite volume point dilution method (FVPDM) test and active distributed temperature sensing (Active-DTS) measurements were conducted in a single piezometer in a chalk aquifer. The FVPDM is a single-well tracer experiment, that provides a measurement of the groundwater flow rate across the tested piezometer. Whereas the Active-DTS method was performed by deploying a fiber-optic (FO) cable outside the piezometer within the gravel filter. The Active-DTS method provided high spatial resolution and local groundwater flux estimates along the heated section. Numerical simulations were used to assess the distortion of the groundwater flow field induced by the presence of the well, demonstrating that the groundwater flux is maximum within the well screen, where the FVPDM test was conducted. In the immediate vicinity of the well, where the heated FO cable was installed, the groundwater flux is lower, and the flow pattern consisted of converging and diverging flow lines. Therefore, the position of the heated FO cable relative to the flow direction is critical and can have a significant impact on the estimation of the groundwater flux. Thus, even if the deployment of the FO cable within the gravel pack minimizes convective effects and opens up interesting perspectives to estimate vertical heterogeneities, this approach may be limited if the position of the FO cable relative to the flow direction is not well known.

**Keywords** Groundwater flux · Tracer tests · Numerical modeling · Flow field distortion · Heterogeneity

## Introduction

Quantifying groundwater fluxes is essential in geothermal and geotechnical engineering for assessing recharge and contaminant transport. The most commonly used approach to estimate groundwater fluxes is based on Darcy's law, which depends on independent estimates of the hydraulic conductivity of the aquifer and the hydraulic gradient. However, this approach provides a spatially averaged estimate of the groundwater flux, whereas local and direct measurements of groundwater flux may be necessary for assessing contaminant transport and planning remediation (Devlin and McElwee 2007). Thus, efforts have been made in the past decades to develop and propose field methods that provide direct estimates of groundwater fluxes.

In this context, point dilution methods (PDMs) have been developed to estimate groundwater flow rate by injecting a tracer (saline or dye) into a piezometer (Drost et al. 1968; Novakowski et al. 2006; Pitrak et al. 2007; Fahrmeier et al. 2020). Among PDMs, the finite volume point dilution method (FVPDM) is a single-well tracer experiment that involves continuously injecting a tracer into a piezometer (Brouyère et al. 2008). During tracer injection, groundwater flow carries the tracer out of the piezometer. Therefore, the higher the groundwater flux, the lower the remaining tracer mass in the piezometer. The FVPDM provides a measurement of the groundwater flow rate along the tested interval (screened length of the piezometer) based on the evolution of tracer concentration. FVPDM tests are performed within piezometers and can be applied in any hydrogeological

✉ Nataline Simon
nataline.simon2@gmail.com

[1] Department Urban and Environmental Engineering, Hydrogeology and Environmental Geology, University of Liege, Building B52, 4000 Sart Tilman, Belgium

[2] Nagaré Tech, University of Liege, Aquapôle, Building B53, 4000 Sart Tilman, Belgium

Published online: 10 July 2024

setting, including both consolidated and unconsolidated aquifers (Brouyère et al. 2008; Goderniaux et al. 2010; Wildemeersch et al. 2014; Dujardin et al. 2014;

Jamin et al. 2015, 2020a). Furthermore, the FVPDM is also well-suited for monitoring transient groundwater flow conditions (Jamin and Brouyère 2018; Jamin et al. 2020b).

Likewise, thermal response tests have been widely developed to estimate groundwater fluxes. Active-DTS measurements rely on distributed temperature sensing (DTS) technology, which provides temperature measurements at high spatial and temporal resolution along a Fiber-Optic (FO) cable (Bense et al. 2016). For Active-DTS measurements, the FO cable is electrically heated, and the temperature elevation measured during heating directly depends on the water flux (Read et al. 2014). The term "Active" refers to the application of an artificial heat source, while the term "Passive-DTS" is commonly used when recording natural temperature variations. The ideal scenario is when Active-DTS is applied in saturated, unconsolidated materials, such as at the groundwater-stream interface (Simon et al. 2022; Banks et al. 2022) or in sandy aquifers (Bakker et al. 2015; des Tombe et al. 2019). In these cases, the FO cable is in direct contact with the porous media. It can be assumed that the installation of the cable does not disrupt the water flow, and an analytical solution can be used to simulate the measured temperature increase during heating. This approach has proven to be efficient in estimating groundwater flux with low uncertainties (Simon et al. 2021).

However, performing Active-DTS measurements in consolidated materials can be challenging. The application of Active-DTS in open boreholes is limited due to thermally driven convection effects caused by active heating (Sellwood et al. 2015a, b; Klepikova et al. 2018). To minimize convection effects, and also to prevent vertical flow within the borehole, some studies have proposed sealing boreholes with flexible borehole liners (Coleman et al. 2015; Maldaner et al. 2019; Munn et al. 2020); however, the installation of borehole liners is time-consuming and does not fully prevent convective effects from occurring within the liner (Pehme et al. 2007). It is also possible to use grout, such as sand, to seal the borehole once the FO cable is installed (Selker and Selker 2018; Maldaner et al. 2021; Zhang et al. 2023); however, in this case, the borehole can no longer be used for other applications.

As the sealing of the borehole is not ideal, it is possible to deploy a heated FO cable outside the well, as proposed by del Val et al. (2021). They applied this approach in a sandy aquifer, which means that the FO cable was in direct contact with both the screen tube and the porous media. Likewise, Godinaud et al. (2023) proposed installing the FO cable outside the well, within the gravel that fills the space between the well and the aquifer. In both cases, Active-DTS measurements are conducted in a fully saturated porous media, which is a necessary condition to use the analytical solution validated by Simon et al. (2021) and estimate the groundwater flux. This configuration is also effective in preventing convective effects. The main issue with this configuration is that the presence of a well induces converging and diverging flow lines in the vicinity of the well (Drost et al. 1968; Kearl 1997; Klammler et al. 2007; Verreydt et al. 2015), which implies that when the FO cable is deployed outside the well, its position relative to the direction of groundwater flow may be a critical point. This critical point has been discussed for Active-DTS tests conducted in open boreholes (Sellwood et al. 2015a) but never studied when the FO cable is deployed outside the well.

Studies often rely on the use of a single method to assess groundwater flux, and the available methods are rarely compared. In this study, both FVPDM and Active-DTS measurements are performed in a consolidated aquifer, within a single piezometer. Concerning Active-DTS, the method is applied by deploying the heated FO cable outside the well and filling the space between the well tube and the aquifer with gravel, which allowed for a discussion of the benefits and limitations of such an approach. Then, the groundwater flux estimated using the FVPDM is compared with the estimates obtained from Active-DTS measurements. The comparison between two field methods may be challenging, especially due to the measurements not necessarily being integrated over similar time and spatial ranges. Indeed, FVPDM provides an estimate of the groundwater flow rate across the piezometer, while Active-DTS measurements provide local and distributed estimates of groundwater fluxes occurring within the filter pack. This provides a discussion on the relative effects of the borehole on the flow field and, consequently, on the representativeness of groundwater flux measured in boreholes.

## Materials and methods

### Background

#### FVPDM

The finite volume point dilution method (FVPDM) is a single-well tracer experiment that involves continuous injection of a tracer (saline or dye) into a piezometer (Brouyère et al. 2008). The approach allows for the measurement of the groundwater flow rate crossing the screen. A recirculation loop is used to ensure the uniform distribution of the tracer within the tested interval. This loop involves installing a mixing pump at the bottom of the tested interval and reinjecting the pumped water at the top (Fig. 1b). A portion of the injected tracer mass is transported out of the well by the groundwater as it flows through the piezometer. Thus, in the case of steady-state flow conditions,

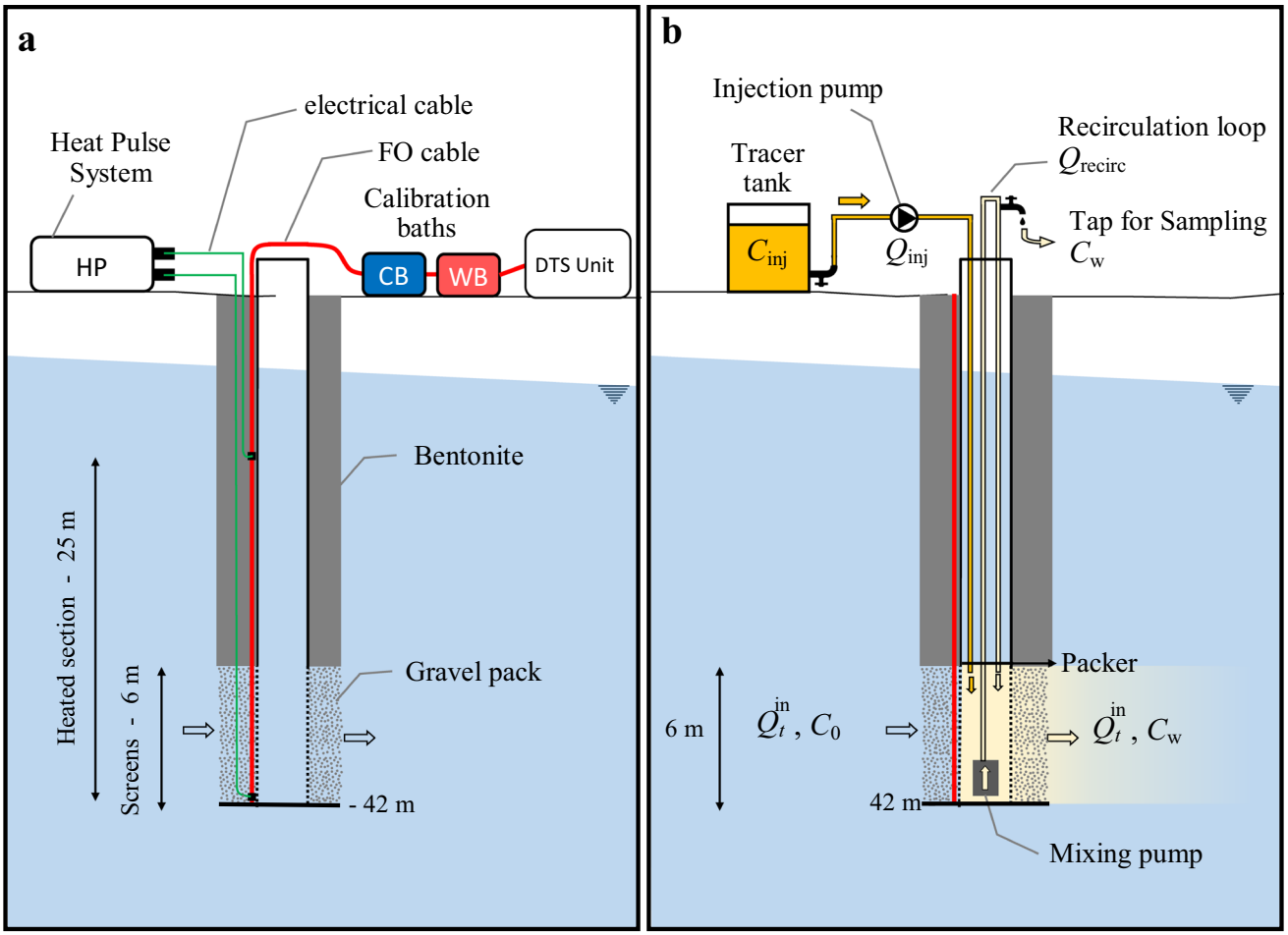


**Fig. 1** Experimental setup of **a** the Active-DTS experiment; **b** the FVPDM test

the concentration of the tracer within the well initially increases during the tracer injection before stabilizing and reaching a plateau at later times. The higher the groundwater flux, the lower the tracer concentration reached during the stabilization stage, as the tracer becomes more diluted by the groundwater flow through the well screen. The increase in tracer concentration within the tested interval depends on several factors, including experimental parameters such as the concentration of the injected water ($C_{inj}$) and the tracer injection flow rate ($Q_{inj}$). Additionally, it is influenced by the flow rate of the groundwater crossing the screen of the injection well ($Q_t^{in}$).

Brouyère et al. (2008) introduced an analytical solution for modelling the evolution of tracer concentration evolution ($C_w$) [$M^1L^{-1}$] measured within the tested interval:

$$C_w(t) = \frac{C_{inj}Q_{inj} + \left[C_0\left(Q_{inj} + Q_t^{in}\right) - C_{inj}Q_{inj}\right]e^{-\frac{\left(Q_{inj}+Q_t^{in}\right)}{V_w}(t-t_0)}}{Q_{inj} + Q_t^{in}} \quad (1)$$

In Eq. (1), $C_{inj}$ and $C_0$ are the tracer concentrations [$M^1L^{-1}$] of the injected water and of the water in the well at $t_0$ respectively. $Q_{inj}$ is the injection flow rate, while $Q_t^{in}$ is the flow rate of groundwater crossing the screen of the injection well [$L^3T^{-1}$], resulting from the hydraulic gradient in the aquifer. The term $V_w$ corresponds to the volume of water in the injection well [$L^3$] and depends on the height of the water column $h_w$ [$L^1$] and on the radius of the piezometer $r_w$ [$L^1$] ($V_w = \pi {r_w}^2 h_w$).

The transit flow rate $Q_t^{in}$ crossing the well screen under injection conditions ($Q_{inj} > 0$) is given by Brouyère (2003):

$$Q_t^{in} = Q_t \sin\left[\arccos\left(\frac{Q_{inj}}{\pi Q_t}\right)\right] - \frac{Q_{inj}}{2\pi}\left[2\arccos\left(\frac{Q_{inj}}{\pi Q_t}\right)\right] \quad (2)$$

For data interpretation, Eq. (1) is first used to reproduce the tracer concentration measured in the field by assessing the optimal value of $Q_t^{in}$. The method allows for the estimation of $Q_t^{in}$, which is the groundwater flow rate occurring through the well under injection conditions. However, the purpose of the test is to assess the groundwater flux

occurring under natural flow conditions. For doing so, Eq. (2) can be used to calculate the transit groundwater flow rate $Q_t$ [$L^3T^{-1}$], which corresponds to the groundwater flow rate occurring through the well under natural flow conditions (no tracer injection, $Q_{inj} = 0$).

Then, the value of the apparent Darcy flux $q_{app}$ can be calculated, depending on the well screen length $e_{scr}$ [L], as follows:

$$q_{app} = \frac{Q_t}{2\,\pi\, r_w e_{scr}} \tag{3}$$

Using the value of $q_{app}$, the Darcy flux components [$LT^{-1}$] at the well radius can be evaluated in a ($r$,$\theta$) coordinate system centered on the well by (Bidaux and Tsang 1991):

$$q_r(r_w, \theta) = -q_{app}\cos\theta \tag{4}$$

### Active-DTS

Another approach that can be used to estimate groundwater fluxes is to perform active distributed temperature sensing (Active-DTS) measurements. The DTS technology provides distributed temperature measurements along fiber optic (FO) cables at high spatial and temporal resolution. The highest-performing DTS systems available provide temperature measurements every second at a 0.125-m sample spacing. In Active-DTS, the FO cable is heated while the thermal response (temperature elevation) is continuously monitored during the heating period. Active-DTS, when conducted in fully saturated porous media, allows for the estimation of the groundwater flux at a high spatial resolution with relatively low uncertainty (Read et al. 2014; Simon et al. 2021).

During the heating period, the observed thermal response can be divided into three stages (Simon et al. 2021; del Val et al. 2021). First, during a short period, the temperature increases rapidly due to heat storage and conduction through the FO cable. Then, when the injected heat reaches the porous material, the conduction-dominant stage begins, during which a gradual increase in temperature is observed. The heat propagation through the porous media is then controlled by conduction. The temperature elevation depends on the thermal properties of the porous media, particularly its thermal conductivity. The higher the thermal conductivity, the lower the temperature increase resulting from the heat injection. Finally, at later times and under flow conditions, the temperature elevation stabilizes, depending on the groundwater flux. This corresponds to the advection-dominant stage, during which the advective groundwater flow dissipates the heat injected into the porous media. Thus, the higher the groundwater flux, the lower the temperature increase resulting from the heat injection. Under no-flow conditions, the temperature continues to increase over time and does not stabilize.

As validated by Simon et al. (2021), the temperature elevation $\Delta T_{PM}$ [$\Theta^1$] observed during both the conduction-dominant and the advection-dominant stages can be modelled using the moving instantaneous line source model (MILS), initially introduced by Carslaw and Jaeger (1959):

$$\Delta T_{PM}(x,y) = \frac{Q}{4\pi\lambda}\exp\left[\frac{qx}{2D_t}\frac{\rho_w c_w}{\rho c}\right]\int_{\frac{x^2+y^2}{4tD_t}}^{\infty}\exp\left[-\Psi-\left(\frac{x^2+y^2}{D_t}\right)\frac{q^2}{16D_t\Psi}\frac{\rho_w^2 c_w^2}{\rho^2 c^2}\right]\frac{d\Psi}{\Psi} \tag{5}$$

With Eq. (5), the thermal response can be modelled all along the line source considering an initial thermal equilibrium ($\Delta T = T - T_0$). The coordinates $x$ and $y$ correspond to the distance [$L^1$] from the heat source, located at $x = 0$ and $y = 0$. $\rho_w c_w$ and $\rho c$ are the volumetric heat capacities of water and of the rock-fluid matrix, respectively [$L^{-1}T^{-2}M^1\Theta^{-1}$]. $D_t$, the thermal diffusivity coefficient [$L^2T^{-1}$], corresponds to the ratio between $\rho c$ and $\lambda$, the bulk thermal conductivity [$L^1T^{-3}M^1\Theta^{-1}$]. $Q$ is the constant and uniform heating rate power [$L^1T^{-3}M^1$] and $q$ is the uniform and constant groundwater flux in the x-direction (or specific discharge) [$L^1T^{-1}$]. The interpretation of the temperature elevation $\Delta T_{PM}$ allows interpretation of the thermal conductivity $\lambda$ and the groundwater flux $q$ for each measurement interval along the heated section.

Simon et al. (2021) validated a two-step method for interpreting the thermal response measured during the heating period. In the first step, the temperature elevation measured during the conduction-dominant stage is modelled using the MILS model (Eq. 5), considering no groundwater flux ($q = 0$). This step provides an estimate of the thermal conductivity of the porous media surrounding the FO cable, as the groundwater flux does not control the temperature rise during this stage. In the second step, the MILS model can be used to reproduce the entire thermal response. Since the groundwater flux controls the behavior of the temperature at later times, this second step allows for estimating the value of the groundwater flux. This approach can be applied to each measurement interval located along the heated section, providing high spatial resolution estimates of both thermal conductivities and groundwater flux values. If there is no temperature stabilization observed at the end of the heating period, this means either that there was no flow at the interval of measurement (only conduction dominated the heat propagation and the temperature kept increasing) or that the heating period was not long enough to reach

the advection-dominant stage. In this case, it is not possible to estimate the effective groundwater flux and the maximum flux occurring ($q_{lim}$) is estimated instead. The value of $q_{lim}$ corresponds to the value of flux below which the measured temperature increase is identical regardless of the value of flux considered. In other words, for any value of $q > q_{lim}$, the advection-dominant stage would be reached, and thus the start of the temperature stabilization period. Considering the large amount of data to be interpreted, the ADTS Toolbox (Simon and Bour 2023), an open-access program, can be used for automatically interpreting Active-DTS measurements.

## Field application

### Experiment site

The experiment was conducted as a part of the CASPER project, which aims to develop an integrated approach for managing pollution risks in peri-urban groundwater catchments (Brouyère et al. 2022). The research site is located within the municipalities of Hornu and Boussu in Wallonia, Belgium. A network of piezometers is used to monitor contaminant mass fluxes within the chalk aquifer of the Mons basin and evaluate the pollution levels impacting the pumping wells that are used for distributing drinking water. Piezometric maps of the area show that groundwater flows from south to north. The hydraulic conductivity of the chalk aquifer varies, ranging between $1 \times 10^{-5}$ m s$^{-1}$ for the coarse chalk and $10^{-7}$ m s$^{-1}$ for fine chalk. The chalk of the Mons Basin is highly fractured and shows faults with metric to decametric spacing. This can greatly increase the hydraulic conductivity of the aquifer, reaching $1 \times 10^{-3}$ m s$^{-1}$ in the fractured areas. Fractures are primarily found at the top of the chalk formation.

The experiment is conducted in piezometer P4 within the Lower Cretaceous chalk aquifer of the Mons basin. P4 was hammer-drilled in November 2022 and features internal and external diameters of 50 and 63 mm, respectively. The external diameter of the borehole along the screened interval is 135 mm. The geological logging of the piezometer shows the presence of brown sand up to 11.5 m depth then clay to 16.5 m depth. Between 16.5 and 20.5 m, the subsurface consists of a mixture of chalk and tuffeau stone (limestone) with flint. From 20.5 m and to the bottom of the piezometer (42 m), the chalk formation is highly fractured. The piezometer is screened between 36 and 42 m depth (Fig. 1), where it is assumed that the groundwater flow is dominated by fractures. Both methods (FVPDM and Active-DTS) were performed in the same piezometer, but measurements were made 1 day apart. As constant piezometric levels were measured during the 2 days of experiments, it is assumed that similar groundwater flow conditions were present for both experiments.

### FVPDM test

Figure 1b shows the experimental setup used for the FVPDM test. The tracer was injected at 36 m depth and the mixing pump was installed at the bottom of the piezometer (42 m). Thus, the tested interval (6 m) matched with the length of the screens. A packer was installed at 36 m-depth to isolate the tested interval. This allowed for a reduction in the mixing volume and the time required to achieve stabilization of tracer concentration (Brouyère et al. 2005). The tracer (KCl) was continuously injected for 4.15 h ($Q_{inj} = 5 \times 10^{-6}$ m$^3$ s$^{-1}$). As the tracer concentration cannot be directly measured in the field, the electrical conductivity was measured instead. This approach is consistent because there is a linear relationship between the concentration of KCl and electrical conductivity (Yun et al. 2009). The tracer consisted of 500 g of KCl dissolved in 100 L of tap water. A conductivity temperature depth (CTD) probe was used to verify that the injected tracer concentration ($C_{inj} = 9.05$ mS cm$^{-1}$) remained constant over time. The tracer concentration ($C_w$) was measured within the recirculation loop using a HACH HQ40d Probe with a precision of 0.5 mS cm$^{-1}$. The recirculation flow rate applied within the tested interval was constant over time and was $Q_{recirc} = 1.58 \times 10^{-4}$ m$^3$ s$^{-1}$.

### Active-DTS

During the installation of piezometer P4, a 3.8-mm diameter Fiber-Optic (FO) cable including 4 multimode 50/125-µm fibers were deployed outside the piezometer tube (Fig. 1a). The space between the tube and the borehole wall was filled with gravel (grain size = 2–4 mm) along the screened interval (6 m) and with bentonite above. Thus, the FO cable was installed within the gravel pack, which helps to minimize convection effects. The FO cable was deployed to be attached to the well screen every 2 m and aligned with the general flow direction observed on regional piezometric maps. In this configuration, the FO cable was perpendicular with respect to horizontal groundwater flow.

Measurements were carried out with an AP Sensing interrogator unit (DTS N4386B), which provided temperature measurements every 25 cm at a 30-s sampling interval. The spatial resolution of the measurement provided by the DTS unit is 50 cm; however, in practice it was probably higher, ranging from 75 cm to 1 m (Tyler et al. 2009; Simon et al. 2020). Data calibration was performed by installing PT100 probes (with an accuracy of ±0.1 °C) in the two calibration baths, with 15 m of FO cable deployed in each. The cold calibration bath was filled with ice, while the warm calibration bath consisted of water heated with an immersion heater, which automatically regulated the temperature of the water (30 °C).

A 25-m section of this cable was electrically isolated (Fig. 1a), and a Heat Pulse Control System (Silixa) was used to inject electricity through the FO cable. Thus, the FO cable was directly heated, and only one cable was used as the heating line source as well as to monitor the distributed temperature. As the hydraulic gradient in the aquifer is low (~0.002 m $m^{-1}$), a relatively small groundwater flux is expected. For low groundwater flux values, longer heating periods are recommended. Long heating periods allow for reaching temperature stabilization, reducing uncertainty in estimating groundwater flux (Simon et al. 2021). The cable was heated for 5 h at a rate of 15.6 $Wm^{-1}$. Likewise, Simon et al. (2021) suggested injecting an electrical power between 15 and 35 $Wm^{-1}$, which is sufficiently high to improve measurement resolution and reduce errors in flux estimates.

The temperature increases measured along the heated section were interpreted with the ADTS Toolbox (Simon and Bour 2023), which relies on the use of the MILS model (Eq. 5). In this case, the application of this model assumes the infinite horizontal extent and the homogeneity of the aquifer, and that the flow is strictly horizontal and perpendicular to the FO cable.

## Numerical model

The presence of wells induces distortion in groundwater flow. This means that converging and diverging flow lines occur near the well (Drost et al. 1968; Kearl 1997; Klammler et al. 2007; Verreydt et al. 2015). It implies that the groundwater flux in the aquifer differs from the groundwater flux within the gravel filter and also differs from the groundwater flux through the well screen. Thus, for Active-DTS measurements, the position of the FO cable within the gravel pack, relative to the flow direction, may be a critical point. Therefore, to facilitate a more accurate comparison of both methods and to evaluate the effect of the FO cable position of flux estimates, a numerical model was relied on for this study. The idea was to simulate the flow distortion, which is the effect of the gravel pack and the well screen on groundwater flow patterns. It should allow for the comparison of the groundwater flowing through the well screen with the groundwater flux in the aquifer, as well as the assessment of the flow distribution around the well.

To account for these distortions, groundwater flow patterns through the borehole were modelled using COMSOL Multiphysics®. The free and porous media flow module was used to estimate water flux through a two-dimensional (2D) model (COMSOL Multiphysics 2020). The aquifer and the gravel filter (radius: 0.076 m) were implemented as porous media with different values of permeability (Fig. 2). As the shape of the screen cannot be easily modelled in a 2D model, the screen (thickness = 0.0046 m; internal radius = 0.0254 m) was also implemented as a porous medium with a high value of hydraulic conductivity. The center of the domain corresponds to the well, where water was implemented as the material (Density $\rho = 1{,}000$ kg $m^{-3}$; Dynamic viscosity $\mu = 1 \times 10^{-3}$ Pa s). The value of groundwater flux within the aquifer, as considered in the numerical model, was calibrated based on the estimated value of groundwater flux obtained from the FVPDM. By considering a value of $q = 2.46 \times 10^{-6}$ m $s^{-1}$ in the aquifer, the water flux simulated within the well is in good agreement with the flux estimated with the FVPDM test (as described in the following).

It is worth noting that the values of hydraulic conductivities (aquifer and gravel) set in the numerical model are approximate estimates. Therefore, the numerical model does not aim to precisely reproduce the effective groundwater fluxes. The model is used to assess the flow field and its distortion around the well. The aim is to understand how representative the estimates of groundwater flux are with

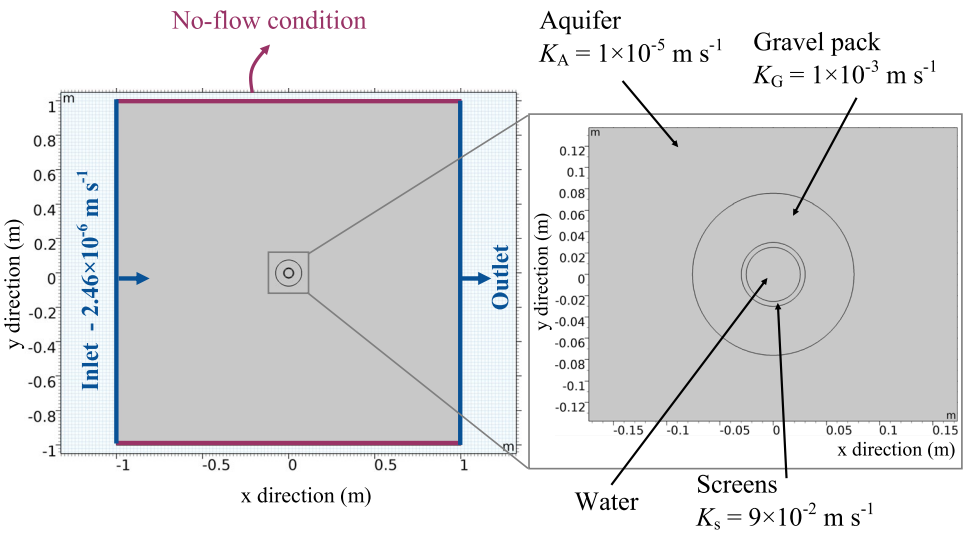


**Fig. 2** Scheme of the numerical model built with COMSOL Multiphysics in order to assess the effect of both the gravel filter and the well on the flow. *K* are values of hydraulic conductivities applied for each element of the model

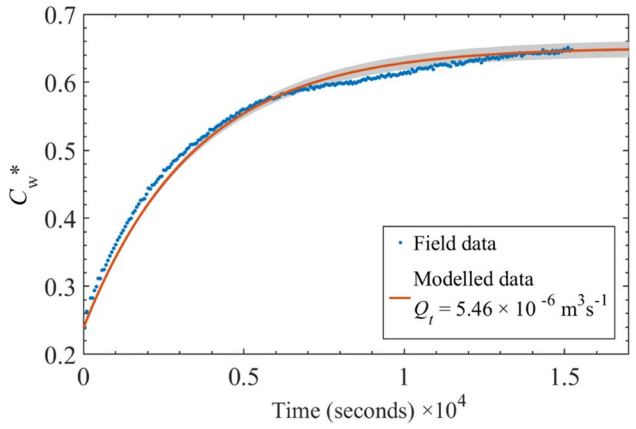


**Fig. 3** Interpretation of the FVPDM test. The grey area reflects the uncertainty of the measurements and accounts for the resolution of the conductivity probe

each method, compared to the actual groundwater flux in the aquifer.

## Results

### Groundwater flow rate measurement with the FVPDM

Figure 3 shows the evolution of the normalized tracer concentration $C_w^* = C_w/C_{inj}$ measured within the well during the FVPDM test (blue dots). The tracer concentration progressively increases until it stabilizes at $C_w^* \approx 0.65$ after approximately 4 hours. The red curve corresponds to the modelled tracer concentration evolution considering a value of groundwater flow rate $Q_t = 5.46 \times 10^{-6}$ m$^3$ s$^{-1}$, which is the optimal value that provides the best fit for field data. By considering the uncertainty of the conductivity probe (resolution 0.1 mS cm$^{-1}$), it can be found that the value of $Q_t$ may vary by ±6% (grey area). Note that the recirculation flow rate is sufficiently high compared to the groundwater flow rate to ensure the perfect mixing of the tracer within the tested interval. This means that Eq. (1) is well-suited for the interpretation of measurements (Simon et al. 2023).

Using Eq. (3), it is possible to calculate the apparent Darcy flux at $q_{app} = 9.58 \times 10^{-6}$ m s$^{-1}$. Due to the flow distortion induced by the well (converging flow lines occurring near the well), the Darcy flux components are not equal around the well radius and can be calculated from Eq. (4) (Fig. 4). The location of the maximal flux around the well depends on the flow direction (at $\Theta = 0$ and $\Theta = \pi$ when the axis [0, π] is oriented in the flow direction). For $\pi/2 < \Theta < 3\pi/2$, the Darcy flow component is positive, indicating that the flow converges towards the well. On the contrary, for $3\pi/2 < \Theta < 5\pi/2$, the Darcy flow component is negative, indicating that the flow diverges from the well. Perpendicular to the flow direction (for $\Theta = \pi/2$ and for $\Theta = 3\pi/2$), the Darcy flow component is zero, indicating that there is no flow entering or leaving the well screen at these points. Note that the groundwater flux calculated using Eq. (2) corresponds to the maximum value of the Darcy flux components around the well (Fig. 4).

### Groundwater flux measurements from Active-DTS

Along the heated section, located along the screened interval (from 73.4 to 79.4 m from the DTS unit), two types of thermal response curves were recorded. First, for certain measurement points, the temperature stabilization was not achieved by the end of the heating period (Fig. 5a). This means either that there was no flow at the point of measurement (only conduction dominated the heat propagation and the temperature kept increasing), or that the heating period was not long enough to reach the advection-dominant stage (stabilization). In this case, it is not possible to estimate the effective groundwater flux; however, it is still possible

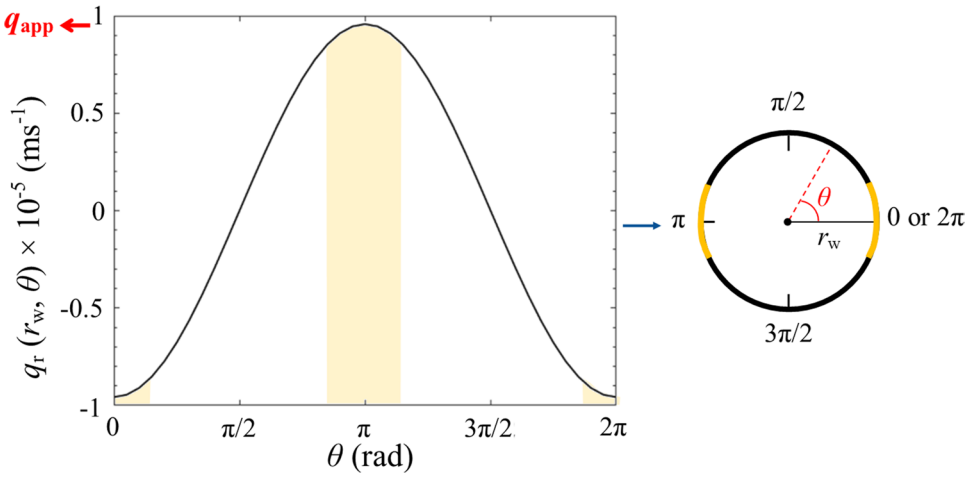


**Fig. 4** Darcy flux components around the well calculated using Eq. (4). The y-axis is oriented in the flow direction. Yellow areas correspond to the surface where the flux component is at least 90% of the absolute value of the maximum flux.

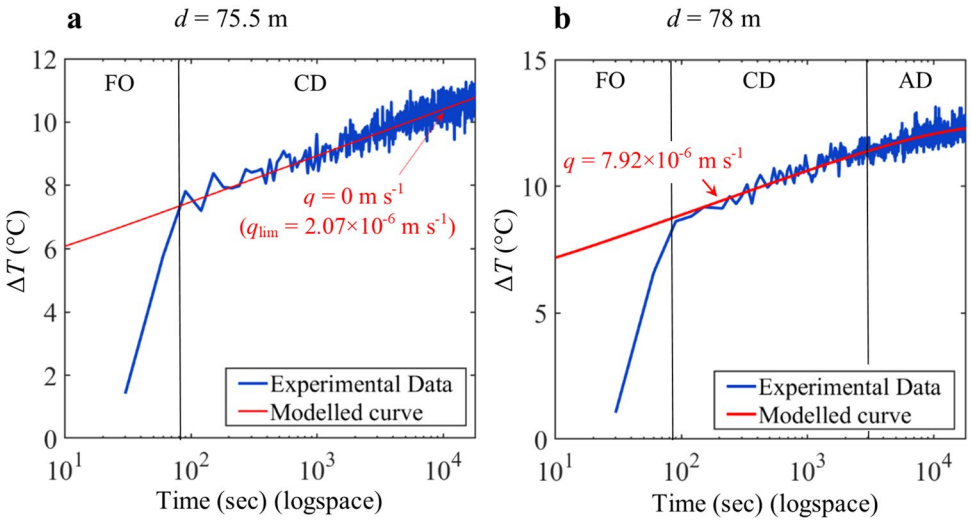


**Fig. 5** Examples of temperature elevations measured during the heating period (blue curves) in case of the temperature stabilization is reached (**b**) or not (**a**). The data are interpreted with the ADTS Toolbox (Simon and Bour 2023), which relies on the MILS model to reproduce field data (red curves). FO: temperature elevation induced by the heating of the FO cable; CD: conduction-dominant stage; AD: advection-dominant stage

to estimate the maximum flux occurring, $q_{lim}$ ($2.07 \times 10^{-6}$ m $s^{-1}$ for this example). Secondly, for most measurement points, the temperature stabilized at later times (Fig. 5b). In this case, it is possible to estimate the value of the groundwater flux ($7.92 \times 10^{-6}$ m $s^{-1}$ for this example). Note that the heating duration applied only enabled recording the beginning of the temperature stabilization period; however, this is sufficient as the data interpretation can be done as soon as the transition between the conduction-dominant period and the advection-dominant period is observed. In both cases, the thermal conductivity was estimated by calculating the slope of the temperature increase measured during the conduction-dominant period (CD), during which the temperature increase is independent of the groundwater flux.

The temperature data is particularly noisy because the performance of the DTS unit used was not optimal for the selected sampling (25 cm) and acquisition time (30 s). The data could be smoothed to reduce the noise. However, it was decided to interpret the raw temperature signals, and the uncertainties on thermal conductivity and groundwater flux estimates were calculated based on this noise. To calculate the uncertainties, the groundwater flux was estimated for an average temperature increase $\Delta T$, as well as for $\Delta T = +0.4$ °C and $\Delta T = -0.4$ °C (with a noise level of ~0.8 °C). This provided minimal and maximal estimates of the groundwater flux.

Figure 6 presents the results of the interpretation of Active-DTS measurements for each measurement point

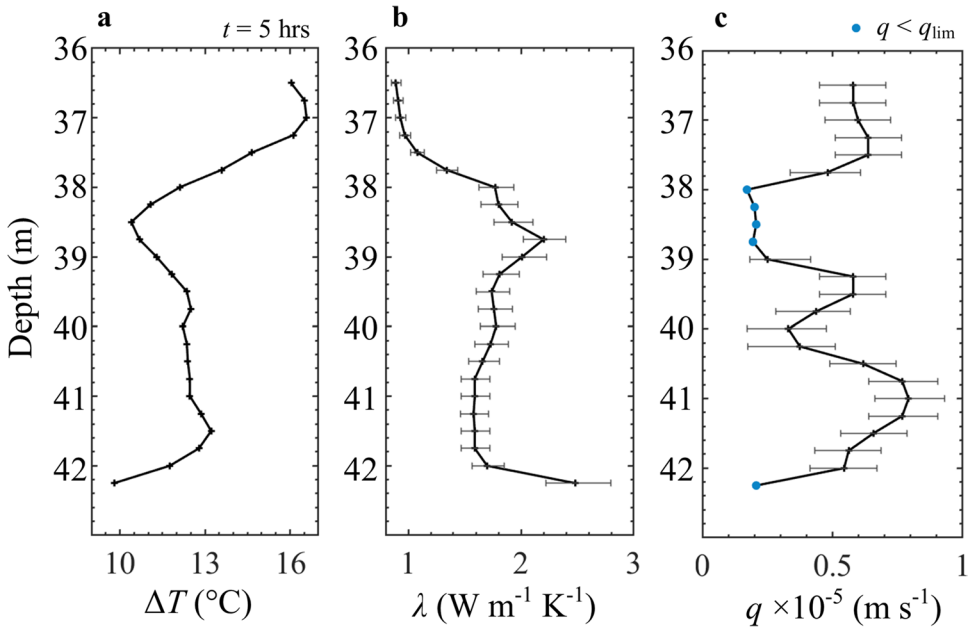


**Fig. 6** Interpretation of the Active-DTS measurements collected along the heated section deployed within the gravel (6 m at the bottom of the well). The distances correspond to the distance from the DTS unit, the bottom of the well is at 79.2 m. **a** Temperature elevation profiles measured at the end of the heating periods (5 h); **b** Profile of estimated values of thermal conductivities; **c** Profile of estimated values of groundwater fluxes

located along the screen. At the end of the heating period, the temperature elevations $\Delta T$ obtained along the heated section deployed within the gravel varied between 9.6 and 16.5 °C (Fig. 6a), with higher temperature elevations measured in the upper part of the screen (up to 37.8 m depth). Note that during the experiment, the mean temperature above the screen was 11.8 °C and did not vary significantly over time with a standard deviation of 0.05 °C. The data interpretation first provided estimates of the thermal conductivity of the surrounding material for each measurement point (Fig. 6b). Low values of thermal conductivity (<1.5 W $m^{-1}$ $K^{-1}$) were found in the upper part of the screen, between 36.5 and 37.5 m depth, while higher values (≈1.7 W $m^{-1}$ $K^{-1}$) were found in the lower part of the screen, from 38 m depth.

The thermal conductivity of saturated gravel varies between 1.6 and 2 W $m^{-1}$ $K^{-1}$ (Stauffer et al. 2013), which is consistent with the values estimated in the lower part of the screen section. However, similar values of thermal conductivity would be expected throughout the screen because the same material (gravel) was used to fill the space between the aquifer and the screen. The lower values of thermal conductivity found in the upper part could potentially be due to a mixture of gravel and bentonite. The thermal conductivity of bentonite ranges between 0.5 and 0.8 W $m^{-1}$ $K^{-1}$. This mixture may have occurred during the filling of the part of the well above the screen with bentonite, as no sand was added above the gravel to reduce the bentonite flowing into the gravel pack. However, this interval (~2 m) may be too long to assume that the low values of thermal conductivity are solely attributed to the mixing of bentonite and sand.

Concerning groundwater flux in the gravel pack, estimates vary between $2.5 \times 10^{-6}$ and $7.92 \times 10^{-6}$ m $s^{-1}$, with a mean value of $4.9 \times 10^{-6}$ m $s^{-1}$. For five measurement points (represented by blue dots), temperature stabilization was not achieved at the end of the heating period, which means that either there is no flow at these measurement points or that the heating period was not sufficient to reach temperature stabilization. Note that the time required to reach temperature stabilization depends on the thermal conductivity value. Here, the five measurement points where the temperature stabilization was not achieved correspond to locations where the values of thermal conductivity are the highest. This result is consistent since the higher the thermal conductivity, the longer the time required to reach temperature stabilization

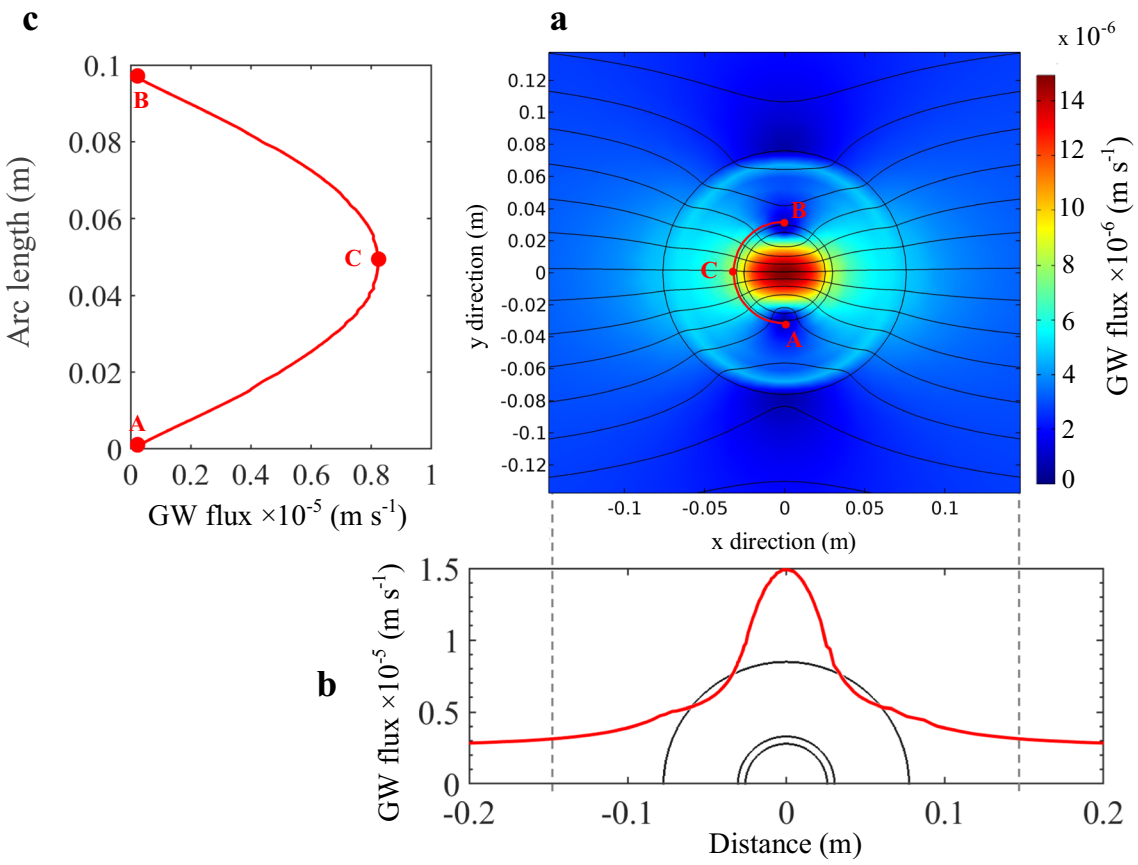


**Fig. 7** Groundwater (GW) flux in **a** the flow field near and within the well; **b** modelled along the x-direction for y = 0 (center); and **c** modelled along the arc A, around the well screen where the FO is installed

(Simon et al. 2021). A longer heating duration may have allowed the temperature to stabilize; however, in this case, it is not possible to estimate the effective groundwater flux and, the value of $q_{lim}$ was calculated as the maximum flux occurring ($q < q_{lim}$) (Simon and Bour 2023).

### Groundwater flow pattern around the well

Figure 7 shows the results of the numerical modelling. The value of groundwater flux estimated through the FVPDM was used to calibrate the value of groundwater flux within the aquifer considered in the numerical model. Thus, by considering a value of $q = 2.5 \times 10^{-6}$ m s$^{-1}$ in the aquifer, the water flux simulated within the well (Fig. 7a) is in good agreement with the groundwater flux estimated with the FVPDM test ($q_{app} = 9.8 \times 10^{-6}$ m s$^{-1}$).

The numerical modeling allows for assessing the distribution of groundwater flow near and within the well. The groundwater flow direction is orthogonal to the y-axis at the boundaries of the model but converges towards the well in the center of the model domain. The gravel filter and the well both have higher hydraulic conductivities relative to the aquifer, which means that the groundwater flux is higher near and within the well along the x-direction for y = 0 (Fig. 7a,b). Around the well screen (Fig. 7c), the groundwater flux is also highly variable. The groundwater flux is maximum along the horizontal flow line (y = 0 flow line). The presence of the well induces converging and diverging flow lines, which implies that the groundwater flux is zero on both sides of the well screen (points A and B).

## Discussion

### Groundwater flux estimates

In regards to interpreting the groundwater flux estimates derived from the two methods, it is critical to understand what each method measures and therefore represents. Groundwater fluxes estimated using both FVPDM and Active-DTS correspond to apparent values of groundwater fluxes as opposed to the effective groundwater flow through the aquifer. The gravel filter and the well both have higher hydraulic conductivities than the aquifer, which results in the groundwater flux being higher near and within the well (Fig. 7a,b).

The heated FO cable is deployed outside the well screen (Fig. 8a). This approach therefore accounts for a local measurement of the groundwater flux that occurs in the gravel. The presence of the well induces converging and diverging flow lines, which impact the groundwater flow pattern around the well (Fig. 7). As the Active-DTS method provides local measurements, Fig. 7 shows that the estimated groundwater flux is maximum when the FO cable is aligned with the centered and horizontal flow line and attached to the well screen (Fig. 8a). This point will be further discussed in the following.

The FVPDM method (Fig. 8b) allows for the measurement of the groundwater flow rate occurring through the well screen. The measurement integrates all groundwater flux components entering the well. The apparent groundwater flux is calculated using the measured groundwater flow rate (Eq. 3). Using Eq. (4), it is possible to calculate the Darcy flux components at the well radius (Fig. 8c). It is interesting to note that the value of the apparent groundwater flux, which is calculated from the measured groundwater flow rate, corresponds to the maximum Darcy flux component found at the well radius for $\Theta = \pi$ and $\Theta = 0$ (see yellow points in Fig. 8b).

A direct comparison of results is difficult due to the groundwater flux estimated with the FVPDM reflecting the integrated average of groundwater flow rate inside the well screen whilst Active-DTS measurements provide an estimate of the groundwater flux outside the well screen

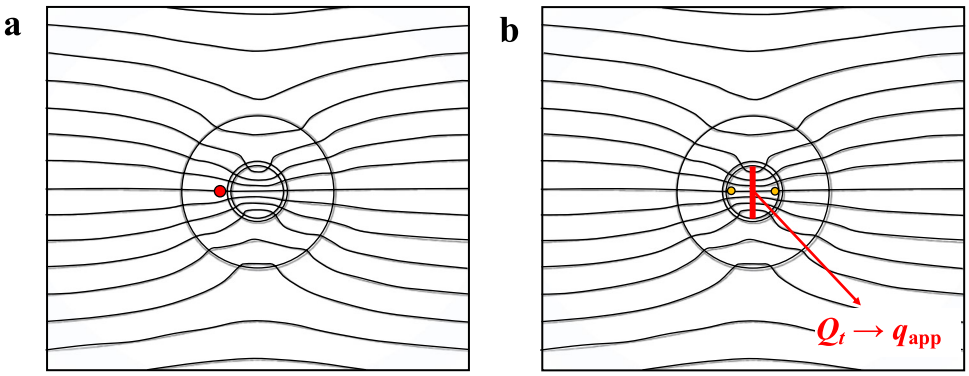


**Fig. 8** Flow patterns around the injection well in natural flow conditions. For Active-DTS measurements, the FO cable (red point) was deployed outside the piezometer screen (**a**) and allowed for the measurement of the local groundwater flux. The FVPDM experiment (**b**) allowed for the measurement of the groundwater flow rate through the piezometer screen. Yellow points depict the location of the maximum Darcy flux components found at the well radius (from Fig. 4)

at point. Along the x-direction (for y = 0), the groundwater flux is higher inside the well than outside the well (Fig. 7b). This means that, even if the FO cable is aligned with the horizontal flow line and attached to the well screen, the groundwater flux estimated with the FVPDM is necessarily higher than the groundwater flux estimated with Active-DTS measurements, which is in perfect agreement with field results. The groundwater flux calculated with the FVPDM ($q_{app} = 9.8 \times 10^{-6}$ m s$^{-1}$) is approximately double the mean groundwater flux estimated from Active-DTS measurement ($\approx 5 \times 10^{-6}$ m s$^{-1}$).

Due to the flow distortion caused by the well, both the FVPDM and the Active-DTS method offer estimates of the "apparent" groundwater flux. For the FVPDM, the effective Darcy flux $q_d$ in the aquifer, which represents the "true" groundwater flux in the aquifer, can be estimated using the flow distortion coefficient $\alpha_w$ (Drost et al. 1968; Brouyère 2003). This coefficient corresponds to the ratio between the apparent water flow rate crossing the screen section and the theoretical (or effective) flow rate that would transit across the same section in the absence of the well ($q_{app} = \alpha_w q_d$). Drost et al. (1968) proposed a formula to estimate the distortion coefficient, which can be applied to any point dilution method result or any measurement method that provides estimates of the groundwater flow rate crossing the screened section. The value of the coefficient depends on the radius and the permeability of the aquifer, the screens, and material(s) used in the filter zone(s). Considering the uncertainties in permeability estimates, using the flow distortion coefficient only provides a rough estimate of the effective groundwater flux in the aquifer. Concerning Active-DTS measurements, only the use of a numerical model can provide an estimate of the effective groundwater flux in the aquifer. At present, there is no formula available for estimating the ratio between the apparent groundwater flow rate in the filter zone and the effective groundwater flux in the aquifer. It should be feasible to propose a formula such as the one suggested by Drost et al. (1968), but this formula would require validation through laboratory experiments.

## About Active-DTS measurements

The results of Active-DTS measurements are consistent with the groundwater flux simulated by the numerical model (Fig. 7). The maximum value of groundwater flux, modelled at point C, is ~$8 \times 10^{-6}$ m s$^{-1}$ which is consistent with the maximum groundwater flux estimated from Active-DTS measurements (~41 m depth). However, the groundwater fluxes estimated elsewhere along the heated section are lower. This can be attributed to subsurface heterogeneities, such as the presence of fractures, which can cause preferential pathways at different depths and vertical variations in horizontal groundwater flux. However, this result can also be attributed to changes in the position of the FO cable in space. Numerical simulations show that the maximum value of groundwater flux is only found at point C, where the cable crosses the central and horizontal flow lines. Elsewhere within the gravel pack, groundwater fluxes are significantly variable in space (in both the x and y directions) due to the distortion of the flow field near the well. Consequently, the groundwater flux measured through Active-DTS measurements depends on both the position of the FO cable within the gravel pack in relation to the flow direction (Fig. 7c), and the distance between the FO cable and the well casing (Fig. 7b). Note also that the interpretation of Active-DTS measurements relies on the assumption that the groundwater flow is perpendicular to the FO cable. This assumption can be questioned, especially when the approach is used in boreholes with a long screened section, where the vertical flow component within the gravel filter may be significant compared to the horizontal flow component. Further developments should be done to fully address the influence of the nonperpendicular flow on the heating response along the heated FO cable.

Here, the FO cable was installed based on the general flow direction observed on regional piezometric maps. In theory, the FO cable is assumed to be installed at point C, aligned with the horizontal flow line and attached to the well screen. In practice, the precise groundwater flow direction near the well is not known and it is impossible to determine the exact position of the FO cable. This lack of knowledge may explain the vertical variability of measured groundwater flux (Fig. 6c).

The position of the FO cable is thus a critical point for the application of Active-DTS in boreholes. These results are in good agreement with the results of Sellwood et al. (2015a), who conducted Active-DTS measurements in an open borehole and showed that the location of measurement within the borehole relative to the borehole center is a potential source of error in borehole flow rates. Here, the installation of the FO cable outside the well screen is an efficient approach to minimize convective heat transfers and avoid the use of borehole liners, which can be time-consuming to install. However, this approach is also constraining and technically challenging because it requires controlling the position of the cable around the well. Note also that it was assumed in this study that the casing and the screen are centered in the borehole. In practice, this might not be the case, and the position of the casing and the screen relative to the center of the borehole might also affect the flow distortion and, thus, the results of Active-DTS measurements.

Calculation of the porous-medium Rayleigh number (Nield and Bejan 2013) confirmed that free thermal convection should be negligible in the present case. This means that the installation of the FO cable outside the well within the gravel pack is an efficient approach to minimize convective

effects. However, the interpretation of the data collected near the boundary conditions of the investigated section should be carefully discussed. The temperature profile measured during the heating period (Fig. 6a) shows the highest temperature increases at the top of the screen. As the impermeable bentonite layer above the gravel filter was also heated, this could have induced a vertical temperature flux from the bentonite layer towards the gravel, which may have contributed to a part of the temperature increase measured at the top of the gravel layer. This hypothesis cannot be experimentally validated, but it remains consistent as the value of $\Delta T$ measured after 5 h of heating is similar in the bentonite layer and at the top of the gravel layer. Likewise, the minimal temperature increase measured at the bottom of the gravel layer may be attributed to the vertical heat dissipation into the bedrock beneath the borehole (Wu et al. 2023). If vertical heat transport occurs within the gravel pack near the boundary conditions, the use of the MILS model is not appropriate because this model does not account for temperature transport along the line source. For further applications of the method, it is recommended to truncate the measurement points located at the top and bottom of the investigated heated section to remove the potential effect of boundary conditions.

The results show that, based on current knowledge, deploying a single FO cable outside a well screen, as done in this study or by del Val et al. (2021) and Godinaud et al. (2023), is not sufficient to accurately assess the groundwater flux in the aquifer. As the installation of the cable and the flow direction are generally uncertain, it is difficult to determine whether the variability in groundwater fluxes measured along the heated section is due to subsurface heterogeneities or changes in the position of the FO cable. The flux component around the well is highly variable (Fig. 4), and the area where at least 90% of the maximum flux can be reliably measured is quite limited. It should also be noted that the location of the FO cable in relation to the flow direction should also be considered when the borehole is sealed (Coleman et al. 2015; Selker and Selker 2018; Maldaner et al. 2019, 2021; Munn et al. 2020; Zhang et al. 2023). This is because the presence of the sealed well inevitably causes a local distortion.

## Conclusion and perspectives

In this study, two single-well tracer experiments for estimating groundwater fluxes in a chalk aquifer were compared. Firstly, the FVPDM provided an estimate of the groundwater flow rate through the well screen, whereas the Active-DTS method provided distributed and local estimates of groundwater fluxes through the gravel filter, outside the well screen. The main advantage of the FVPDM is that it can be applied to existing piezometers; however, investigating subsurface heterogeneities with the FVPDM requires the use of packers which is particularly time-consuming. Likewise, unlike Active-DTS, the FVPDM is not well-suited for boreholes with long screened sections, and the physical and chemical properties of the groundwater (such as density, turbidity, etc.) can impact the accuracy of FVPDM results.

Concerning Active-DTS measurements, the position of the FO cable is a critical point due to the high flow distortion around the well. Further investigations should be conducted to more accurately evaluate the impact of flow direction in relation to the position of the FO cable. For now, it is still challenging to determine whether the spatial variations in groundwater flux measured along the heated section are caused by subsurface heterogeneities or by shifts in the position of the FO cable. To better control this, a solution could be to install multiple heated FO cables around the well screen or to wrap the FO cable around it. Such a configuration would also allow for a better assessment of the flow direction.

Consequently, assessing the position of the FO cable related to the flow direction is absolutely necessary for the right interpretation of Active-DTS measurements performed in wells. This ensures that the groundwater flux estimate is representative of the aquifer groundwater flux value, which is an important result as it shows that the use of the Active-DTS method outside the well may be questioned if the position of the FO cable relative to the groundwater flow is uncertain. However, if the position of the FO cable related to the flow direction is well known, the Active-DTS method may provide valuable insights for the characterization of groundwater flow dynamics. In this case, the approach is efficient for characterizing the distribution of groundwater flux and its vertical variability at high spatial resolution. To minimize convective heat transfers, the heatable FO cable must be installed in direct contact with a porous medium. In this study, installing the FO cable outside the well screen and filling the space between the aquifer material and the screen with gravel was proposed. This approach avoids the need to seal the borehole or use flexible borehole liners. With this configuration, and if the position of the FO cable is well known, the well can be used for other applications such as measuring pollutant concentrations and assessing contaminant mass fluxes, which is essential for characterizing polluted sites. In addition, the permanent installation of an FO cable allows for repeated surveys under different hydrological conditions, as well as a more detailed characterization of the spatial and temporal variability of mass fluxes.

This study clearly shows the advantages and limitations of each method. It emphasizes that, while both methods aim to estimate the groundwater flux, the results of the estimates depend on the experimental conditions, including the spatial resolution of measurements. This study questions the ability to measure groundwater flux in the field and highlights the

difficulty of obtaining a representative estimate of groundwater flux. Lastly, results show that both methods are complementary. While the FVPDM allows for the assessment of the groundwater flux in short screens, Active-DTS measurements provide distributed estimates of flux and can be applied in long-screened boreholes or highly permeable aquifers. Both methods are well-suited for assessing the mass fluxes of contaminants, which is a crucial element in the management of polluted soils.

**Acknowledgements** The authors would like to thank Pascal Goderniaux and Louis Christiaens (Mons University), and Samuel Wildemeersch and Eric Vandenberghe (SPAQuE) for loaning the equipment required for conducting FVPDM measurements.

**Funding** Nataline Simon is a beneficiary of the IPD-STEAM fellowship supported by the Special Funds for Research. This work is supported by the FNRS Belgium (grant No. J.0023.22). The CASPER Project has been supported by the SPGE (Société Publique de Gestion de l'Eau) (grant No. DF08).

## Declarations

**Conflicts of Interest** On behalf of all authors, the corresponding authors state that there is no conflict of interest.

**Open research** Data to support the findings for this research (field results) are available on the ULiège Open Data Repository : https://doi.org/10.58119/ULG/J4XLJJ (Simon et al. 2024).

## References

Bakker M, Calje R, Schaars F, et al (2015) An active heat tracer experiment to determine groundwater velocities using fiber optic cables installed with direct push equipment. Water Resour Res 51:2760–2772. https://doi.org/10.1002/2014WR016632

Banks EW, Morgan LK, Sai Louie AJ, et al (2022) Active distributed temperature sensing to assess surface water–groundwater interaction and river loss in braided river systems. J Hydrol 615:128667. https://doi.org/10.1016/j.jhydrol.2022.128667

Bense VF, Read T, Bour O, et al (2016) Distributed temperature sensing as a downhole tool in hydrogeology. Water Resour Res 52:9259–9273. https://doi.org/10.1002/2016WR018869

Bidaux P, Tsang C-F (1991) Fluid flow patterns around a well bore or an underground drift with complex skin effects. Water Resour Res 27:2993–3008. https://doi.org/10.1029/91WR01947

Brouyère S (2003) Modeling tracer injection and well-aquifer interactions: a new mathematical and numerical approach. Water Resour Res 39. https://doi.org/10.1029/2002WR001813

Brouyère S, Balzani L, Orban P (2022) The CASPER project: an integrated approach for pollution risk assessment in peri-urban groundwater catchment areas. Adv Geosci 59:45. https://doi.org/10.5194/adgeo-59-45-2022

Brouyère S, Batlle-Aguilar J, Goderniaux P, Dassargues A (2008) A new tracer technique for monitoring groundwater fluxes: the finite volume point dilution method. J Contam Hydrol 95:121–140. https://doi.org/10.1016/j.jconhyd.2007.09.001

Brouyère S, Carabin G, Dassargues A (2005) Influence of injection conditions on field tracer experiments. Ground Water 43:389–400. https://doi.org/10.1111/j.1745-6584.2005.0041.x

Carslaw HS, Jaeger JC (1959) Conduction of heat in solids. Oxford University Press, Oxford, UK

Coleman TI, Parker BL, Maldaner CH, Mondanos MJ (2015) Groundwater flow characterization in a fractured bedrock aquifer using active DTS tests in sealed boreholes. J Hydrol 528:449–462. https://doi.org/10.1016/j.jhydrol.2015.06.061

COMSOL Multiphysics® v. 5.6. (2020) COMSOL AB, Stockholm, Sweden. www.comsol.com. Accessed June 2024

del Val L, Carrera J, Pool M, et al (2021) Heat dissipation test with fiber-optic distributed temperature sensing to estimate groundwater flux. Water Resour Res 57:e2020WR027228. https://doi.org/10.1029/2020WR027228

des Tombe BF, Bakker M, Smits F, et al (2019) Estimation of the variation in specific discharge over large depth using distributed temperature sensing (DTS) measurements of the heat pulse response. Water Resour Res 55:811–826. https://doi.org/10.1029/2018WR024171

Devlin JF, McElwee CD (2007) Effects of measurement error on horizontal hydraulic gradient estimates. Groundwater 45:62–73. https://doi.org/10.1111/j.1745-6584.2006.00249.x

Drost W, Klotz D, Koch A, et al (1968) Point dilution methods of investigating ground water flow by means of radioisotopes. Water Resour Res 4:125–146. https://doi.org/10.1029/WR004i001p00125

Dujardin J, Anibas C, Bronders J, et al (2014) Combining flux estimation techniques to improve characterization of groundwater–surface-water interaction in the Zenne River, Belgium. Hydrogeol J 22:1657–1668. https://doi.org/10.1007/s10040-014-1159-4

Fahrmeier N, Goeppert N, Goldscheider N (2020) Comparative application and optimization of different single-borehole dilution test techniques. Hydrogeol J. https://doi.org/10.1007/s10040-020-02271-2

Goderniaux P, Brouyère S, Gutierrez A, Baran N (2010) Multi-tracer tests to evaluate the hydraulic setting of a complex aquifer system (Brévilles spring catchment, France). Hydrogeol J. https://doi.org/10.1007/s10040-010-0633-x

Godinaud J, Klepikova M, Larroque F, et al (2023) Clogging detection and productive layers identification along boreholes using active distributed temperature sensing. J Hydrol 617:129113. https://doi.org/10.1016/j.jhydrol.2023.129113

Jamin P, Brouyère S (2018) Monitoring transient groundwater fluxes using the Finite Volume Point Dilution Method. J Contam Hydrol 218:10–18. https://doi.org/10.1016/j.jconhyd.2018.07.005

Jamin P, Cochand M, Dagenais S, et al (2020a) Direct measurement of groundwater flux in aquifers within the discontinuous permafrost zone: an application of the finite volume point dilution method near Umiujaq (Nunavik, Canada). Hydrogeol J 28:869–885

Jamin P, Cosme F, Briers P, et al (2020b) Innovative contaminant mass flux monitoring in an aquifer subject to tidal effects. Groundw Monit Remediat 40:28–39. https://doi.org/10.1111/gwmr.12366

Jamin P, Goderniaux P, Bour O, et al (2015) Contribution of the finite volume point dilution method for measurement of groundwater fluxes in a fractured aquifer. J Contam Hydrol 182:244–255. https://doi.org/10.1016/j.jconhyd.2015.09.002

Kearl PM (1997) Observations of particle movement in a monitoring well using the colloidal borescope. J Hydrol 200:323–344. https://doi.org/10.1016/S0022-1694(97)00026-7

Klammler H, Hatfield K, Annable MD, et al (2007) General analytical treatment of the flow field relevant to the interpretation of passive fluxmeter measurements. Water Resour Res 43. https://doi.org/10.1029/2005WR004718

Klepikova M, Roques C, Loew S, Selker J (2018) Improved characterization of groundwater flow in heterogeneous aquifers using granular polyacrylamide(PAM) gel as temporary grout. Water Resour Res 54. https://doi.org/10.1002/2017WR022259

Maldaner CH, Munn JD, Coleman TI, et al (2019) Groundwater flow quantification in fractured rock boreholes using active distributed temperature sensing under natural gradient conditions. Water Resour Res 55:3285–3306. https://doi.org/10.1029/2018WR024319

Maldaner CH, Munn JD, Green BA, et al (2021) Quantifying groundwater flow variability in a poorly cemented fractured sandstone aquifer to inform in situ remediation. J Contam Hydrol 241:103838. https://doi.org/10.1016/j.jconhyd.2021.103838

Munn JD, Maldaner CH, Coleman TI, Parker BL (2020) Measuring fracture flow changes in a bedrock aquifer due to open hole and pumped conditions using active distributed temperature sensing. Water Resour Res 56:e2020WR027229. https://doi.org/10.1029/2020WR027229

Nield DA, Bejan A (2013) Convection in porous media, 4th edn. Springer, Heidelberg, Germany

Novakowski K, Bickerton G, Lapcevic P, et al (2006) Measurements of groundwater velocity in discrete rock fractures. J Contam Hydrol 82:44–60. https://doi.org/10.1016/j.jconhyd.2005.09.001

Pehme P, Parker BL, Cherry JA, Greenhouse JP (2007) The potential for compromised interpretations when based on open borehole geophysical data in fractured rock. https://www.cluin.org/products/siteprof/2007fracrock/073Molson,J.pdf. Accessed June 2020

Pitrak M, Mares S, Kobr M (2007) A simple borehole dilution technique in measuring horizontal ground water flow. Groundwater 45:89–92. https://doi.org/10.1111/j.1745-6584.2006.00258.x

Read T, Bour O, Selker JS, et al (2014) Active-distributed temperature sensing to continuously quantify vertical flow in boreholes. Water Resour Res 50:3706–3713. https://doi.org/10.1002/2014WR015273

Selker F, Selker JS (2018) Investigating water movement within and near wells using active point heating and fiber optic distributed temperature sensing. Sensors 18. https://doi.org/10.3390/s18041023

Sellwood SM, Hart DJ, Bahr JM (2015) An in-well heat-tracer-test method for evaluating borehole flow conditions. Hydrogeol J 23:1817–1830. https://doi.org/10.1007/s10040-015-1304-8

Sellwood SM, Hart DJ, Bahr JM (2015) Evaluating the use of in-well heat tracer tests to measure borehole flow rates. Groundw Monit Remediat 35:85–94. https://doi.org/10.1111/gwmr.12134

Simon N, Bour O (2023) An ADTS toolbox for automatically interpreting active distributed temperature sensing measurements. Groundwater 61:215–223. https://doi.org/10.1111/gwat.13172

Simon N, Bour O, Lavenant N, et al (2020) A comparison of different methods to estimate the effective spatial resolution of FO-DTS measurements achieved during sandbox experiments. Sensors 20. https://doi.org/10.3390/s20020570

Simon N, Bour O, Lavenant N, et al (2021) Numerical and experimental validation of the applicability of Active-DTS experiments to estimate thermal conductivity and groundwater flux in porous media. Water Resour Res 57:e2020WR028078. https://doi.org/10.1029/2020WR028078

Simon N, Bour O, Faucheux M et al (2022) Combining passive and active distributed temperature sensing measurements to locate and quantify groundwater discharge variability into a headwater stream. Hydrol Earth Syst Sci 26:1459–1479. https://doi.org/10.5194/hess-26-1459-2022

Simon N, Brouyère S, Jamin P (2023) A new discrete model to better consider tracer distribution along boreholes during the Finite Volume Point Dilution Method. J Contam Hydrol 257:104203. https://doi.org/10.1016/j.jconhyd.2023.104203

Simon N, Balzani L, Brouyère S, Jamin P (2024) Data of the paper "Estimating the groundwater flux through Active-DTS (heat tracer experiment) and FVPDM (tracer experiment): a field comparison" (Hydrogeology Journal). ULiège Open Data Repository. https://doi.org/10.58119/ULG/J4XLJJ

Stauffer F, Bayer P, Blum P, et al (2013) Thermal use of shallow groundwater. CRC, Boca Raton, FL

Tyler SW, Selker JS, Hausner MB, et al (2009) Environmental temperature sensing using Raman spectra DTS fiber-optic methods. Water Resour Res 45:W00D23. https://doi.org/10.1029/2008WR007052

Verreydt G, Bronders J, Van Keer I, et al (2015) Groundwater flow field distortion by monitoring wells and passive flux meters. Groundwater 53:933–942. https://doi.org/10.1111/gwat.12290

Wildemeersch S, Jamin P, Orban P, et al (2014) Coupling heat and chemical tracer experiments for estimating heat transfer parameters in shallow alluvial aquifers. J Contaminant Hydrol 169:90–99. https://doi.org/10.1016/j.jconhyd.2014.08.001

Wu X, Kueper B, Novakowski K (2023) Insight into heat dissipation in fractured rock influenced by groundwater influx and heat source configurations using numerical analysis. J Contam Hydrol 257:104219. https://doi.org/10.1016/j.jconhyd.2023.104219

Yun M-H, Yeon J-W, Hwang J, et al (2009) A calibration technique for an Ag/AgCl reference electrode utilizing the relationship between the electrical conductivity and the KCl concentration of the internal electrolyte. J Appl Electrochemy 39:2587–2592. https://doi.org/10.1007/s10800-009-9955-6

Zhang B, Gu K, Bayer P, et al (2023) Estimation of groundwater flow rate by an actively heated fiber optics based thermal response test in a grouted borehole. Water Resour Res 59:e2022WR032672. https://doi.org/10.1029/2022WR032672